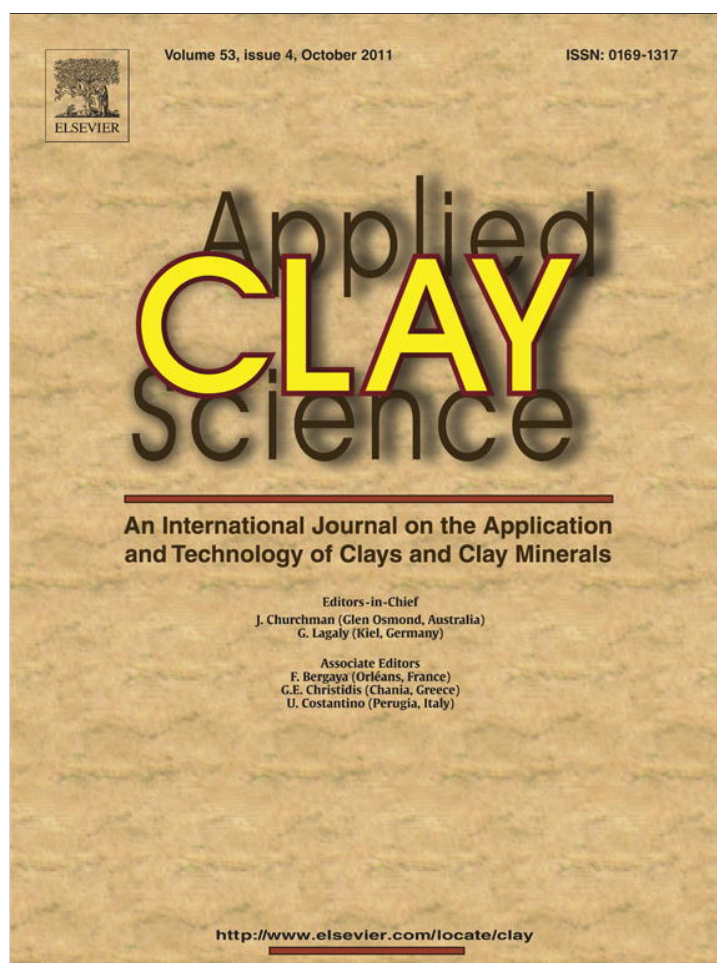


Provided for non-commercial research and education use.  
Not for reproduction, distribution or commercial use.



This article appeared in a journal published by Elsevier. The attached copy is furnished to the author for internal non-commercial research and education use, including for instruction at the authors institution and sharing with colleagues.

Other uses, including reproduction and distribution, or selling or licensing copies, or posting to personal, institutional or third party websites are prohibited.

In most cases authors are permitted to post their version of the article (e.g. in Word or Tex form) to their personal website or institutional repository. Authors requiring further information regarding Elsevier's archiving and manuscript policies are encouraged to visit:

<http://www.elsevier.com/copyright>



Contents lists available at ScienceDirect

Applied Clay Science

journal homepage: [www.elsevier.com/locate/clay](http://www.elsevier.com/locate/clay)

Research Paper

Synthesis and catalytic activity of Ni<sup>0</sup>-acid activated montmorillonite nanoparticlesDipanka Dutta <sup>a</sup>, Bibek Jyoti Borah <sup>a</sup>, Lakshi Saikia <sup>a</sup>, Madan Gopal Pathak <sup>b</sup>,  
Pinaki Sengupta <sup>a</sup>, Dipak Kumar Dutta <sup>a,\*</sup><sup>a</sup> Materials Science Division, North East Institute of Science and Technology (CSIR), Jorhat, Assam-785 006, India<sup>b</sup> Analytical Chemistry Division, North East Institute of Science and Technology (CSIR), Jorhat, Assam-785 006, India

## ARTICLE INFO

## Article history:

Received 25 August 2010

Received in revised form 19 May 2011

Accepted 20 May 2011

## Keywords:

Ni<sup>0</sup>-nanoparticles

Montmorillonite

Nanopores

Face centered cubic lattice

Transfer hydrogenation

## ABSTRACT

Ni<sup>0</sup>-nanoparticles of 0–8 nm were prepared in situ by impregnation of Ni(CH<sub>3</sub>COO)<sub>2</sub> into the nanopores of modified montmorillonite (Mt) followed by polyol reduction. The Mt was activated with HCl under controlled condition for generating desired pore sizes. The porous materials were characterized by XRD, TEM, SEM, UV–visible spectroscopy, FTIR and XPS analysis. N<sub>2</sub> adsorption data revealed specific surface areas (BET) in the range of 296–548 m<sup>2</sup>/g, specific pore volumes of 0.4–0.6 cm<sup>3</sup>/g and pore diameters of 0–6.8 nm. XRD pattern of Ni<sup>0</sup>-nanoparticles revealed the formation of face centered cubic (fcc) lattice. These supported Ni<sup>0</sup>-nanoparticles show efficient catalytic activity in transfer hydrogenation of acetophenone to 1-phenylethanol with about 98% conversion, having nearly 100% selectivity.

© 2011 Elsevier B.V. All rights reserved.

## 1. Introduction

Metal nanoparticles have attracted great attention in recent time for their unique size dependent properties and applications in the fields of catalysis, optoelectronics, magnetic devices, sensors, drug delivery etc. (Campelo et al., 2009; Rao et al., 2000). Recently, much attention has been paid on synthesizing metal nanoparticles with controlled morphology (Puntes et al., 2001; Sun et al., 2000). Nickel nanoparticles are widely used as catalyst (Mahata et al., 2009; Sapkal et al., 2009), soft magnetic materials (Qin et al., 1999), chemically protective coating (Chen et al., 2006), electrodes (Tu et al., 2006) and low temperature super plastic materials (Mcfadden et al., 1999). The stabilizers for synthesizing nanoparticles play an important role in controlling nano size, shape as well as morphology and the most commonly used stabilizers are surfactants (Chen and Hsieh, 2002), polymers (Sharma et al., 2009a), organic ligands (Tamura and Fujihara, 2003), alkylammonium salts (Aiken and Finke, 1999) etc. Among porous materials, silica beads (Kim et al., 2002), zeolites (Campelo et al., 2008), resins (Pande et al., 2008), activated carbon (Mahata et al., 2008), metal oxides (Kantam et al., 2008), and clay minerals (Ahmed and Dutta, 2003a; Kiraly et al., 1996; Sharma et al., 2009b) are utilized for the stabilization of precious metal nanoparticles. Attempts were made to stabilize metal nanoparticles into the interlamellar space of clay minerals of the smectite group like montmorillonite (Mt), hectorite, saponite, etc. (Ahmed and Dutta,

2003a, 2003b; Kiraly et al., 1996; Malla et al., 1991). Metal nanoparticles supported on micro- and mesoporous materials are expected to behave very differently from the unsupported one. Acid activated Mt exhibits high surface area and contained micro- and mesopores which were advantageously utilized for stabilizing metal nanoparticles (Borah et al., 2010; Komadel and Madejova, 2006; Sharma et al., 2009b).

The reduction of carbonyl compounds to the corresponding alcohols is an important organic transformation in the industrial synthesis of dyes, pharmaceuticals, agrochemicals and biologically active compounds (Larock, 1989). Among different routes, transfer hydrogenation is advantageously applied for the reduction for several reasons: (a) the hydrogen donor (isopropanol) is cheap, safe, highly selective and eco-friendly, (b) transfer hydrogenation reaction does not require any elaborate experimental set up or high pressure reactor. A wide variety of homogenous metal complexes have been reported for transfer hydrogenation reaction (Backvall, 2002; Deb et al., 2009; Samec et al., 2006), however, there are few reports (Mohapatra et al., 2002; Upadhyaya et al., 1997) of heterogeneous catalysts with several advantages over homogeneous systems in respect of easy recovery, recycling, enhanced stability and minimization of undesired toxic waste. Alonso et al. (2008a, 2008b) have recently employed nickel nanoparticles for transfer hydrogenation of carbonyl compound to corresponding alcohol by using isopropanol as hydrogen donors. However, such a heterogeneous process need to be improved because of the use of high amount of nickel (10–20 mol%) and the catalyst are not sufficiently stabilized in solution. Moreover, due to stringent and growing environmental regulations, chemical industry needs the development of ecofriendly processes. In view of

\* Corresponding author. Tel.: +91 376 2370 081; fax: +91 376 2370 011.  
E-mail address: [dipakkrdutta@yahoo.com](mailto:dipakkrdutta@yahoo.com) (D.K. Dutta).

the above, we report the in situ generation of Ni<sup>0</sup>-nanoparticles into micro- and mesopores of environmentally benign modified Mt and their catalytic performance in transfer hydrogenation reactions.

## 2. Experimental

### 2.1. Materials and methods

Bentonite (procured from Gujarat, India) contains silica sand, iron oxide etc. as impurities and was purified by dispersion followed by sedimentation technique (Gillott, 1968) to collect the <2 μm fraction. Air dried samples were characterized by XRD and the basal spacing ( $d_{001}$ ) value was found to be 12.5 Å. Specific surface area as determined by N<sub>2</sub> adsorption was 101 m<sup>2</sup>/g. The oxide compositions of the Mt as determined by wet chemical and flame photometric methods were SiO<sub>2</sub>: 49.42%; Al<sub>2</sub>O<sub>3</sub>: 20.02%; Fe<sub>2</sub>O<sub>3</sub>: 7.49%; MgO: 2.82%; CaO: 0.69%; LOI: 17.51%; Na<sub>2</sub>O: 1.05%; K<sub>2</sub>O: 0.62% and TiO<sub>2</sub>: 0.38%.

Mt was converted to the homoionic Na<sup>+</sup>-exchanged form by stirring in 2 M NaCl solution for about 78 h, washed and dialyzed against distilled water until the conductivity of the water approached that of distilled water. To determine the cation exchange capacity, 0.5 g Mt was treated during 24 h with 10 ml of standard alcoholic CaCl<sub>2</sub> solution (0.05 M). The dispersion was filtered and washed repeatedly with alcohol. The washed filtrates were collected in a 250 ml volumetric flask and the volume was made up to the mark with distilled water. The amount of Ca<sup>2+</sup> was determined by titrating by a standard EDTA solution. The difference between the concentration of Ca<sup>2+</sup> before and after exchange corresponds to the CEC (meq/g) of the clay mineral.

The reagents were procured from Acros Organic, Belgium, and used as received without further purification.

FTIR studies were conducted by using a Perkin-Elmer system 2000 FT-IR spectrophotometer. UV-visible absorption spectra were obtained at room temperature by the UV-visible spectrophotometer model Shimadzu 1601 PC, using aqueous dispersion. Powder X-ray diffractions were acquired on a Rigaku, Ultima IV X-ray diffractometer from 2–80° 2θ using CuKα source (λ = 1.54 Å). Specific surface area (BET), specific pore volume and average pore diameter were measured by using Autosorb-1 (Quantachrome, USA). Prior to adsorption at 77 K, the samples were degassed at 250 °C for 3 h. Pore size distributions were derived from desorption isotherms at P/P<sub>0</sub> value of >0.35 and using Barrett-Joyner-Halenda (BJH) method. Scanning Electron Microscopy (SEM) images and energy dispersive X-ray spectroscopy (EDX) patterns were obtained by Leo 1430 vp operated at 3 and 10 KV on gold coated sample. Transmission Electron Microscopy (TEM) images were recorded by a JEOL JEM-2011 electron microscope on isopropanol dispersed samples using a carbon coated grid. X-ray photoelectron spectroscopy (XPS) experiments were performed with a Kratos ESCA model Axis 165 spectrophotometer having a position sensitive detector and hemispherical energy analyzer in an ion pumped chamber. The amount of Ni content was determined by Atomic Absorption Spectrophotometer (AAS) (Model: A Analyst, -700).

### 2.2. Preparation of support

Mt (5 g) was taken into a 250 ml three necked round bottom flask and 100 ml of 4 M hydrochloric acid was added to it. The resulting dispersion was refluxed for 1 and 2 h. After cooling, the supernatant liquid was discarded and the Mt was repeatedly washed with deionized water until free from Cl<sup>-</sup> ion (AgNO<sub>3</sub> test). The clay was recovered, dried in an air oven at 50 ± 5 °C over night to obtain the solid product. These modified Mt were designated as Acid-Mt1 and Acid-Mt2 corresponding to activation time of 1 and 2 h.

### 2.3. Preparation of Ni<sup>0</sup>-nanoparticles

0.5 g of each Acid-Mt1 and Acid-Mt2 were taken separately into 100 ml beakers and 10 ml (0.041 M) aqueous solution of Ni (CH<sub>3</sub>COO)<sub>2</sub> was added slowly to each sample under vigorous stirring condition. The stirring was continued for another 6 h followed by evaporation to dryness in a rotary evaporator. The dry clay-Ni (CH<sub>3</sub>COO)<sub>2</sub> composite was dispersed in 50 ml ethylene glycol in a double necked round bottom flasks and was refluxed at 196 °C for 6 h in nitrogen environment under stirring condition. The products were recovered, washed with methanol until free from ethylene glycol and then dried under nitrogen environment at about 40 °C for 12 h. The samples thus prepared were designated as Ni<sup>0</sup>-1 and Ni<sup>0</sup>-2 corresponding to Acid-Mt1 and Acid-Mt2 supports respectively.

### 2.4. Catalytic transfer hydrogenation of ketones

In a typical reaction, 0.23 ml (2 mmol) of acetophenone, 20 ml of isopropanol, 25 mg (0.02 mmol) of the catalyst (Ni<sup>0</sup>-I or Ni<sup>0</sup>-II) and about 15 mg of NaOH were taken into a two necked round bottom flask of 50 ml capacity and allowed to reflux at 349 K for 2 and 4 h under nitrogen atmosphere. The insoluble catalyst was separated by simple filtration and the product was analyzed by gas chromatography (Chemito 8510) using BP-20 Wide bore capillary column, 30 m × 0.53 mm id × 1.0 μm film thickness and hydrogen as carrier gas.

## 3. Results and discussion

### 3.1. Characterization of support

#### 3.1.1. X-ray diffraction studies

The XRD patterns of Mt before and after acid activation treatment were shown in Fig. 1. The significant structural modification of Mt was reflected by their relative intensity and location of basal spacing ( $d_{001}$ ). The unactivated Mt exhibited an intense peak at 7.06° 2θ, corresponding to a basal spacing ( $d_{001}$ ) of 12.5 Å. On the other hand, Acid-Mt1 showed a decrease in the intensity of this peak and no basal spacing ( $d_{001}$ ) was observed for Acid-Mt2 which indicated non-organization of layers in the C direction. A low intense broad peak in the range of 20–30° 2θ suggested the formation of amorphous silica (Wang et al., 2006).

#### 3.1.2. Specific surface area and pore size distribution

The acid activated Mt showed micro- (<2 nm) and mesopores (2–50 nm) with the pore diameters in the range of 0–6 nm, a high specific surface area up to 548 m<sup>2</sup>/g and specific pore volume of 0.60 cm<sup>3</sup>/g (Table 1). Acid activation leads to modification of layered

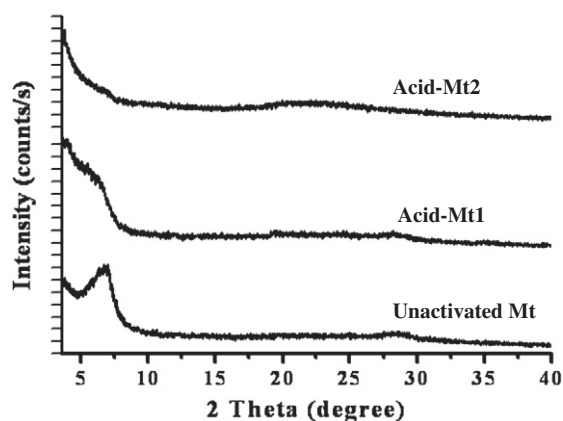


Fig. 1. Powder XRD pattern of different Mt before and after acid activation.

**Table 1**

Surface properties of Mt before and after Ni<sup>0</sup>-nanoparticles loading, cation exchange capacities (CEC) and amount of Ni<sup>0</sup> loading.

Samples	Specific surface area (m <sup>2</sup> /g)	Average pore diameter (nm)	Specific pore volume (cm <sup>3</sup> /g)	CEC (meq./g clay)	Ni (±0.5 wt.%)
Unactivated Mt	101.0	9.16	0.2323	1.26	–
Acid-Mt1	548.0	4.14	0.5970	0.41	–
Acid-Mt2	412.0	6.01	0.6042	0.20	–
Ni <sup>0</sup> -1	315.0	5.20	0.4127	–	4.85
Ni <sup>0</sup> -2	296.0	6.80	0.5460	–	4.85

Mt structure by leaching out aluminum from their tetrahedral and octahedral sites (Bhorodwaj and Dutta, 2010).

The adsorption–desorption isotherms (Fig. 2) of Acid-Mt1 and Acid-Mt2 were of type-IV isotherm with a H3 hysteresis loop at P/P<sub>0</sub> of ~0.4–0.8, indicating mesoporous solids (Gregg and Sing, 1982). The plot of differential volumes against pore diameters (Fig. 3) indicated relatively narrow pore size distribution with an average pore diameter of 4.14 and 6.01 nm for Acid-Mt1 and Acid-Mt2 respectively. These modified clay mineral with high specific surface area and controlled pores in the nano range may be advantageously utilized for in situ generation of Ni<sup>0</sup>-nanoparticles.

### 3.1.3. FTIR study

The FTIR study of acid activated Mt was helpful in estimating the degree of dissolution of layered structure. The unactivated Mt exhibited intense absorption band at ~1034 cm<sup>-1</sup> for Si–O stretching vibrations of tetrahedral layer and bands at 522 and 460 cm<sup>-1</sup> are due to Si–O–Al and Si–O–Si bending vibrations respectively (Fig. 4). With increase in acid activation time, the band at ~1034 cm<sup>-1</sup> shifted to ~1083 cm<sup>-1</sup>, indicating the changes to the bonding environment in tetrahedral layer and appeared a pronounced band near 800 cm<sup>-1</sup>, characteristic of amorphous silica (Komadel and Madejova, 2006; Wallis et al., 2007). The unactivated Mt also showed absorption bands at 3633 and 1645 cm<sup>-1</sup> due to stretching and bending vibrations of OH groups of Al–OH. The bands at 917, 875 and 792 cm<sup>-1</sup> were related to AlAl–OH, AlFe–OH and AlMg–OH vibrations respectively (Komadel and Madejova, 2006; Wallis et al., 2007). The gradual decrease in intensity of these bands with increasing acid activation time indicated the removal of Al, Fe and Mg ions from the clay mineral matrix.

### 3.1.4. SEM-EDX study

SEM-EDX studies of Mt before and after acid activation were shown in Fig. 5. The Acid-Mt2 (Fig. 5c) showed the formation of pores on the surface while those were absent on the unactivated Mt

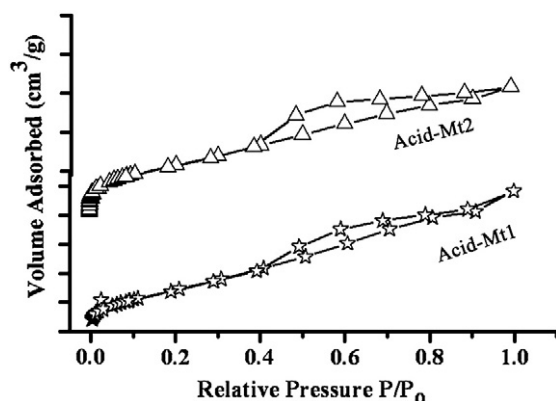


Fig. 2. N<sub>2</sub> adsorption/desorption isotherms of different acid activated Mt.

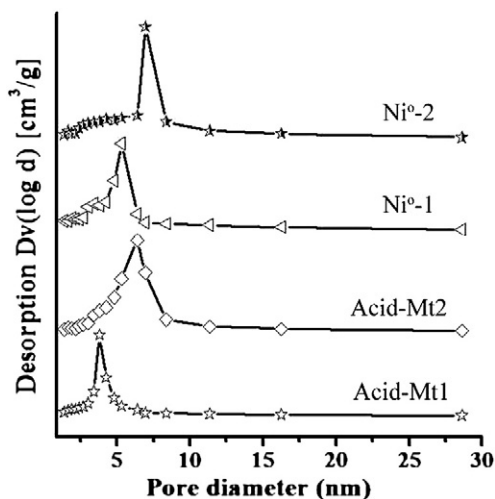


Fig. 3. BJH pore size distribution curves of acid activated Mt before and after Ni<sup>0</sup>-nanoparticles deposition.

(Fig. 5a). Furthermore, EDX spectra (Fig. 5b and d) revealed that upon acid activation the Al content on the clay mineral surface decreased and Si content increased.

### 3.1.5. Cation exchange capacity (CEC)

The CEC of the unactivated Mt (Table 1) i.e. 1.26 meq/g of clay decreases to 0.41 and 0.20 meq/g of clay upon acid activation for 1 and 2 h respectively. This decrease in CEC values is due to the destruction of layered structure of the Mt as the acid activation time increases (Bhorodwaj and Dutta, 2010) and thus substantiates the finding of XRD study.

### 3.2. Characterization of supported Ni<sup>0</sup>-nanoparticles

A preliminary study conducted on the formation of Ni<sup>0</sup>-nanoparticles by UV–visible spectroscopy which showed that the visible absorption band (Fig. 6) observed in the range 630–780 nm due to Ni<sup>2+</sup>-Mt. (before reduction) disappeared for Ni<sup>0</sup>-1 and Ni<sup>0</sup>-2 composites (after reduction) and thus may indicate the formation of Ni<sup>0</sup>-nanoparticles (Dhakshinamoorthy and Pitchumani, 2008).

The TEM images (Fig. 7) and corresponding particles size histograms (Fig. 8) of Ni<sup>0</sup>-1 and Ni<sup>0</sup>-2 revealed the formation of different sizes of Ni<sup>0</sup>-nanoparticles depending upon the micro- and mesopores of Mt generated during acid activation for different time periods. It was evident that the average particle size distribution of Ni<sup>0</sup>-nanoparticles corresponds to the samples Ni<sup>0</sup>-1 and Ni<sup>0</sup>-2 were 1–5 and 4–8 nm respectively. The micrographs clearly indicated that the particles have a spherical morphology and are well dispersed on the support. From

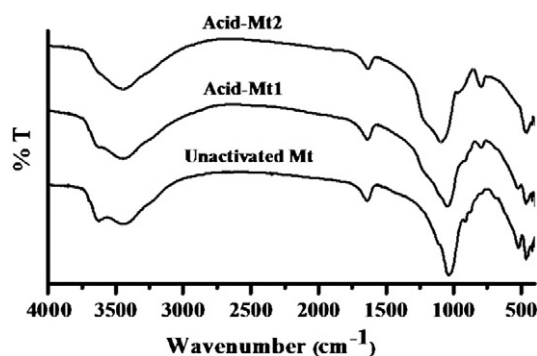


Fig. 4. FTIR spectra of different Mt before and after acid activation.

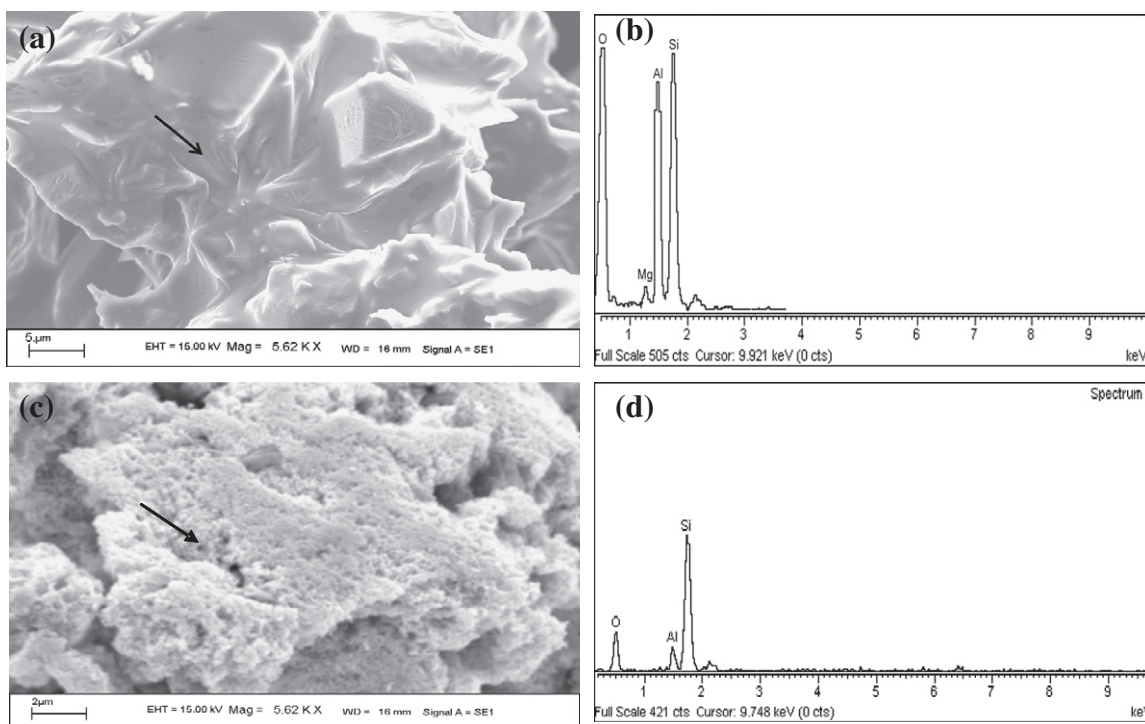


Fig. 5. SEM image of the surface of (a) the unactivated Mt (b) the Acid-Mt2; and EDX analysis of (c) the unactivated Mt and (d) the Acid-Mt2.

TEM study, it was also observed that, some of the Ni<sup>0</sup>-nanoparticles were found to be larger than the pore size of the support which may be due to the presence of Ni<sup>0</sup>-nanoparticles on the outer surface of the support rather than inside the pores. SEM-EDX analysis also substantiated the formation of Ni<sup>0</sup>-nanoparticles on the well-tuned pores of the acid activated Mt (Fig. 9a) with spherical morphology and even distribution throughout the support. Furthermore, EDX analysis (Fig. 9b) confirmed the presence of nickel as the only element in the pores of the support.

The powder XRD of a typical sample Ni<sup>0</sup>-2 showed (Fig. 10) three sharp peaks of 2θ values at 44.5, 51.8 and 76.4° which were assigned to the (111), (200) and (222) indices of face centered cubic (fcc) of metallic Ni (Sharma et al., 2009b). The average crystallite size of Ni<sup>0</sup>-II was calculated for (111) plane and found to be 15 nm. In order to ascertain the oxidation state, the samples were characterized by XPS analysis (Fig. 11) wherein, Ni2p<sub>3/2</sub> photoelectron peak at 852.8 eV with typical doublet separated by 17.2 eV was observed which are in good agreement with the metallic Ni (Hoffer et al., 2003; Wang et al., 2003). However, the other peaks appearing at the higher binding energy may be due to the presence of oxidized Ni (Fig. 11). The

amounts of Ni content in the catalysts were determined by AAS analysis and found to be 4.85 wt.% (Table 1).

It is interesting to mention here that after supporting Ni<sup>0</sup>-nanoparticles on acid activated Mt, the specific surface area and specific pore volume of the clay mineral decrease, while pore diameters were

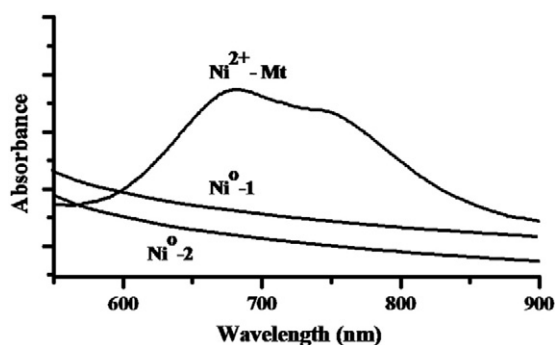


Fig. 6. UV-visible spectra of Ni<sup>2+</sup>-Mt, Ni<sup>0</sup>-1 and Ni<sup>0</sup>-2.

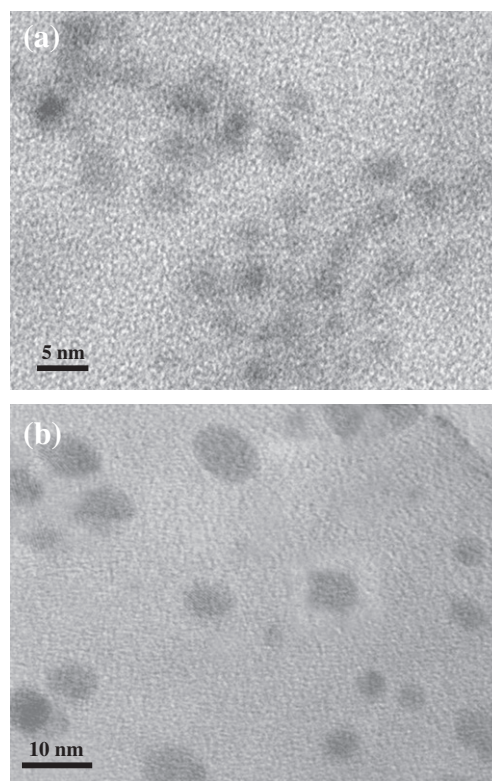


Fig. 7. Representative TEM images of (a) Ni<sup>0</sup>-1 and (b) Ni<sup>0</sup>-2.

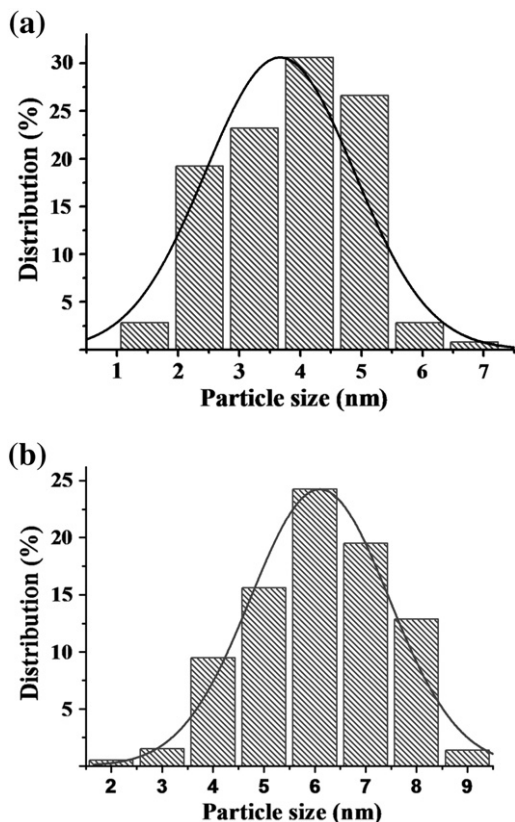


Fig. 8. Particle size histograms of (a) Ni<sup>o</sup>-1 and (b) Ni<sup>o</sup>-2.

found to increase (Table 1). The decrease in specific surface area and specific pore volume may be attributed to the physical occupancy by Ni<sup>o</sup>-nanoparticles into the internal pores. However, increase of pore

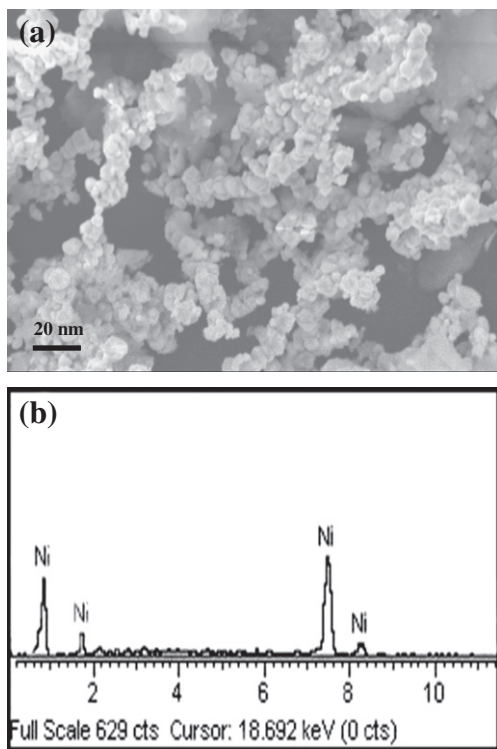


Fig. 9. (a) SEM image of Ni<sup>o</sup>-2 and (b) EDX spot analysis on pores.

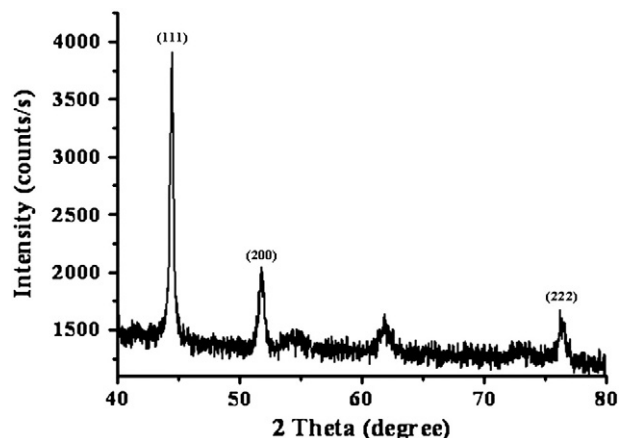


Fig. 10. Powder XRD pattern of Ni<sup>o</sup>-2.

diameter may be due to rupture of some smaller pores to generate bigger ones during the formation of Ni<sup>o</sup>-nanoparticles into the pores. Moreover, the introduction of Ni<sup>o</sup>-nanoparticles into the clay matrix may cause complexities in porosity measurement with nitrogen adsorption, because the electrostatic forces between an adsorbate (i.e. nitrogen) and metallic surface may affect the measured values to some extent. From the distribution curve it showed that both the samples Ni<sup>o</sup>-1 and Ni<sup>o</sup>-2 have a narrow pore size distribution in the range of 0–8 nm (Fig. 3).

### 3.3. Catalytic transfer hydrogenation of acetophenone

The catalytic activities of Ni<sup>o</sup>-1 and Ni<sup>o</sup>-2, containing about 4.85 wt.% Ni, were carried out in transfer hydrogenation reaction of acetophenone to 1-phenylethanol in the presence of isopropanol and NaOH (Scheme 1). The catalysts Ni<sup>o</sup>-1 and Ni<sup>o</sup>-2 showed conversions about 17 and 21% respectively after 1 h reaction time, which enhanced to 92 and 98%, with nearly 100% selectivity on increasing the reaction time to 4 h (Fig. 12).

The high conversion and selectivity shown by the catalysts may be due to high specific surface area and highly dispersed Ni<sup>o</sup>-nanoparticle into the porous matrix of the support. The higher catalytic activity of Ni<sup>o</sup>-2 over Ni<sup>o</sup>-1 may be attributed to the effect of wider specific pore volume of the catalyst matrix. In order to obtain more detail information on the conversion of acetophenone to 1-phenylethanol catalyzed by the highly active Ni<sup>o</sup>-2 catalyst, a thorough investigation was carried out and the results were shown in Fig. 13. It appears that

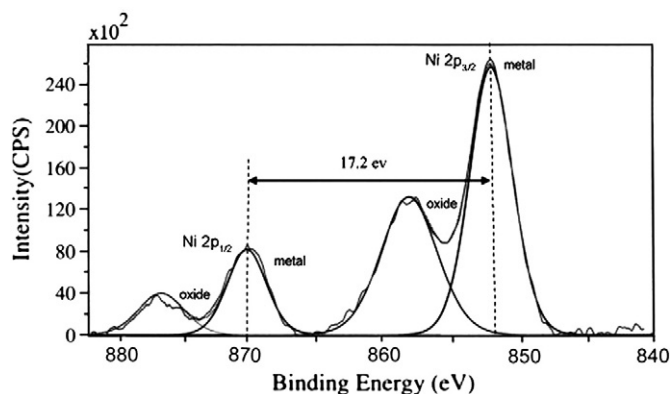
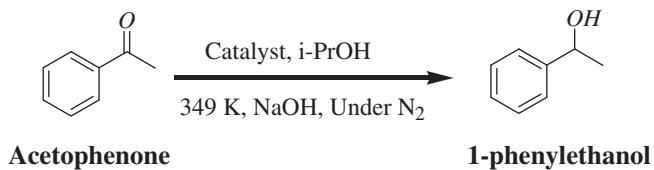


Fig. 11. XPS spectrum of Ni<sup>o</sup>-2.



Scheme 1..

the catalytic conversion proceeds very fast up to a period of 4 h and there after slows down and maintained a constant conversion of 99.3% after 5 h, with nearly 100% selectivity. The catalysts showed very low activity when the reaction was performed in the absence of the base at 349 K; while addition of the base exhibited a beneficial effect with a significant increase in conversion by manifold. A negligible amount of product is formed when the reaction was carried out in presence of base without catalyst. It may be indicated that the acid activated Mt support alone did not show any catalytic activity. The mechanism of the catalytic reaction may follow the well established mono- or dihydride route (Alonso et al., 2008a, 2008b; Ukisu and Miyadera, 1997). It is interesting to mention here that the Raney nickel under the present catalytic reaction condition produced the hydrogenolysis product (Andrews and Pillai, 1978) instead of 1-phenylethanol from acetophenone. Since, the catalyst is susceptible to be oxidized by air, their preparation and subsequent catalytic reactions should be carried out in the absence of oxygen. The effect of amount of catalyst on acetophenone conversion catalyzed by the highly active Ni<sup>0</sup>-2 is shown in Fig. 14. The conversion increased with the increase in the amount of catalyst used for the reactions and also observed that higher the time of reaction, higher is the conversion. The conversion of 31 and 69% shown by 0.005 mmol of catalyst for 2 and 4 h reaction time respectively, enhanced correspondingly to 52 and 98% upon increasing the amount of catalyst to 0.02 mmol. This observation may be attributed to the presence of more active sites for the reactants. The selectivity remained nearly 100% in all cases.

### 3.3.1. Reversibility of the hydrogenation of acetophenone

During the hydrogenation of acetophenone, a decrease in the amount of acetophenone (Table 2) was observed with the progress of the reaction time and after 5 h, a constant amount i.e. 0.7% of acetophenone was observed up to 6 h. On the other hand, if the reaction was carried out in a reverse direction i.e. by starting with 1-phenylethanol under similar reaction condition, it appeared that 0.4% of acetophenone forms immediately and remained almost constant for several hours. Thus, the reaction of acetophenone to 1-phenylethanol is reversible. Similar observation was also reported earlier by Masson et al., 1997.

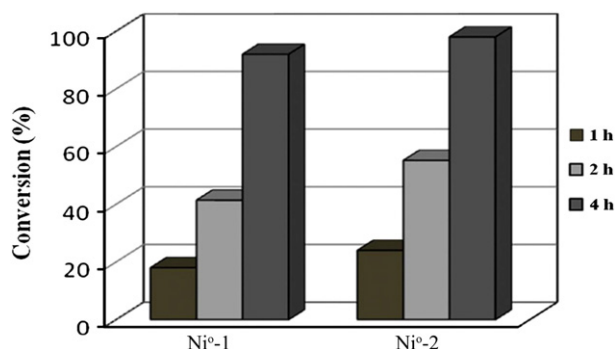


Fig. 12. Effects of different catalysts on transfer hydrogenation of acetophenone. Reaction conditions: acetophenone (2 mmol), NaOH (15 mg) and catalyst (0.02 mmol) in isopropanol (20 ml); Conversion (%) were determined by gas chromatography, selectivity was 100%.

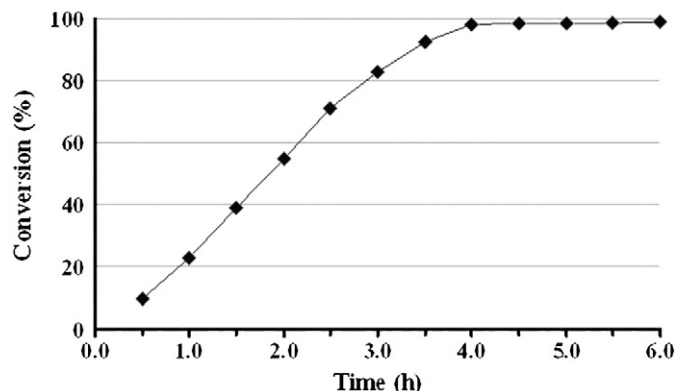


Fig. 13. Effects of reaction time on transfer hydrogenation of acetophenone using Ni<sup>0</sup>-2 catalyst. Reaction conditions: acetophenone (2 mmol), NaOH (15 mg) and catalyst (0.02 mmol) in isopropanol (20 ml); Conversion (%) were determined by gas chromatography, selectivity was 100%.

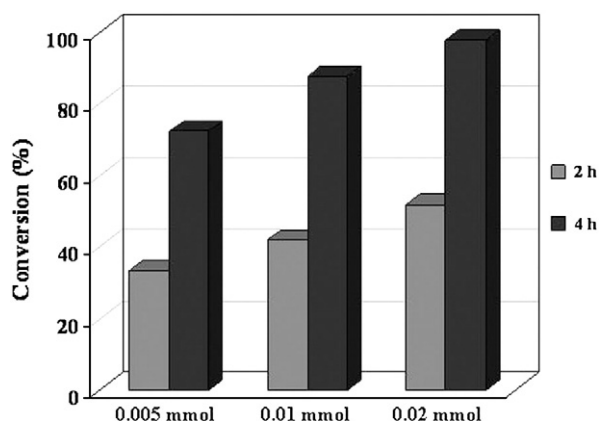


Fig. 14. Effects of catalyst amount on transfer hydrogenation of acetophenone using Ni<sup>0</sup>-2. Reaction conditions: acetophenone (2 mmol) and NaOH (15 mg) in isopropanol (20 ml); Conversion (%) were determined by gas chromatography, selectivity was 100%.

### 3.3.2. Recyclability of the catalyst

In order to regenerate a catalyst like Ni<sup>0</sup>-2 after 4 h reaction, the catalyst was separated by filtration, washed with deionized water, dried in a dessicator and reused for transfer hydrogenation with fresh reaction mixture up to the third run. The results (Table 3) showed a decrease in conversion upon subsequent reuse i.e. the conversion of 98% in the first run decreases to about 87% in the second run and to 64% in the third run, however, the selectivity remained almost unchanged i.e. >99%. This decrease in catalytic activity may be due to leaching of Ni<sup>0</sup>-nanoparticles from the clay support during the catalytic reaction as substantiated by AAS study.

Table 3  
Transfer hydrogenation of acetophenone using recovered catalyst Ni<sup>0</sup>-2.

Run	Conversion (%)	Selectivity (%)
1	98	100
2	87	>99
3	64	>99

Table 2  
Amount of acetophenone left out as a function of reaction time catalyzed by Ni<sup>0</sup>-2.

Time (h)	2	4	5	5.5	6
Acetophenone (%)	48	2	1.2	0.7	0.7

#### 4. Conclusion

Ni<sup>0</sup>-nanoparticles of 0–8 nm generated in situ into the micro- and mesopores of Mt show efficient catalysis in transfer hydrogenation of acetophenone to 1-phenylethanol with conversion of about 98%, having nearly 100% selectivity within a reaction period of 4 h. The high conversion and selectivity of the product may be attributed to the high dispersion and small sizes of the Ni<sup>0</sup>-nanoparticles. The catalysts can be regenerated and reused for several runs.

#### Acknowledgments

The authors are grateful to Dr. P. G. Rao, Director, North East Institute of Science and Technology (CSIR), Jorhat, Assam, India, for his kind permission to publish the work. Thanks are also given to CSIR, New Delhi for a financial support (Network project NWP 0010). Thanks are also due to Dr. M. Lakshmi Kantam, Scientist, IICT, Hyderabad for arranging the XPS experiment. The author BJB is grateful to CSIR for providing the Senior Research Fellowship.

#### References

- Ahmed, O.S., Dutta, D.K., 2003a. In situ generation of metal clusters in interlamellar spacing of Montmorillonite clay and their thermal behaviour. *Thermochimica Acta* 395, 209–216.
- Ahmed, O.S., Dutta, D.K., 2003b. Generation of metal nanoparticles on montmorillonite K 10 and their characterization. *Langmuir* 19, 5540–5541.
- Aiken III, J.D., Finke, R.G., 1999. Polyoxoanion- and tetrabutylammonium-stabilized Rh (0)<sub>n</sub> nanoclusters: unprecedented nanocluster catalytic lifetime in solution. *Journal of the American Chemical Society* 121, 8803–8810.
- Alonso, F., Riente, P., Yus, M., 2008a. Hydrogen-transfer reduction of carbonyl compounds promoted by nickel nanoparticles. *Tetrahedron* 64, 1847–1852.
- Alonso, F., Riente, P., Yus, M., 2008b. Hydrogen-transfer reduction of carbonyl compounds catalysed by nickel nanoparticles. *Tetrahedron Letters* 49, 1939–1942.
- Andrews, M.J., Pillai, C.N., 1978. Hydrogen transfer reactions: part VII—Hydrogen transfer reactions catalysed by raney nickel. *Indian Journal of Chemistry B* 16, 465–468.
- Backvall, J.E., 2002. Transition metal hydrides as active intermediates in hydrogen transfer reactions. *Journal of Organometallic Chemistry* 652, 105–111.
- Bhorodwaj, S.K., Dutta, D.K., 2010. Heteropoly acid supported modified Montmorillonite clay: an effective catalyst for the esterification of acetic acid with sec-butanol. *Applied Catalysis A: General* 378, 221–226.
- Borah, B.J., Dutta, D., Dutta, D.K., 2010. Controlled nanopore formation and stabilization of gold nanocrystals in acid-activated montmorillonite. *Applied Clay Science* 49, 317–323.
- Campelo, J.M., Conesa, T.D., Gracia, M.J., Jurado, M.J., Luque, R., Marinas, J.M., Romero, A.A., 2008. Microwave facile preparation of highly active and dispersed SBA-12 supported metal nanoparticles. *Green Chemistry* 10, 853–858.
- Campelo, J.M., Luna, D., Luque, R., Marinas, J.M., Romero, A.A., 2009. Sustainable preparation of supported metal nanoparticles and their applications in catalysis. *ChemSusChem* 2, 18–45.
- Chen, D.H., Hsieh, C.H., 2002. Synthesis of nickel nanoparticles in aqueous cationic surfactant solutions. *Journal of Materials Chemistry* 12, 2412–2415.
- Chen, Z., Ng, A., Yi, J., Chen, X., 2006. Multi-layered electroless Ni–P coatings on powder-sintered Nd–Fe–B permanent magnet. *Journal of Magnetism and Magnetic Materials* 302, 216–219.
- Deb, B., Borah, B.J., Sarmah, B.J., Das, B., Dutta, D.K., 2009. Dicarboxylruthenium(II) complexes of diphosphine ligands and their catalytic activity. *Inorganic Chemistry Communications* 12, 868–871.
- Dhakshinamoorthy, A., Pitchumani, K., 2008. Clay entrapped nickel nanoparticles as efficient and recyclable catalysts for hydrogenation of olefins. *Tetrahedron Letters* 49, 1818–1823.
- Gillott, J.E., 1968. *Clay in Engineering Geology* First ed. Elsevier, Amsterdam. (Chapter 5).
- Gregg, S.J., Sing, K.S.W., 1982. *Adsorption, Surface Area and Porosity* Second ed. Academic Press Inc., London and New York. (Chapter 3).
- Hoffer, B.W., Crezee, E., Devred, F., Mooijman, P.R.M., Slof, W.G., Kooyman, P.J., VanLangeveld, A.D., Kapteijn, F., Moulijn, J.A., 2003. The role of the active phase of Raney-type Ni catalysts in the selective hydrogenation of D-glucose to D-sorbitol. *Applied Catalysis A: General* 253, 437–452.
- Kantam, M.L., Chakravarti, R., Pal, U., Sreedhar, B., 2008. Nanocrystalline magnesium oxide-stabilized Palladium(0): an efficient and reusable catalyst for selective reduction of nitro compounds. *Advanced Synthesis & Catalysis* 350, 822–827.
- Kim, S.W., Kim, M., Lee, W.Y., Hyeon, T., 2002. Fabrication of hollow palladium spheres and their successful application to the recyclable heterogeneous catalyst for Suzuki coupling reactions. *Journal of the American Chemical Society* 124, 7642–7643.
- Kiraly, Z., Dekany, I., Mastalir, A., Bartok, M., 1996. *In Situ* generation of palladium nanoparticles in smectite clays. *Journal of Catalysis* 161, 401–408.
- Komadel, P., Madejova, J., 2006. Acid activations of clay minerals. In: Bergaya, F., Theng, B.K.G., Lagaly, G. (Eds.), *Handbook of Clay Science*. : Developments in Clay Science, vol. 1. Elsevier, Amsterdam, pp. 263–271 (Chapter 7.1).
- Larock, R.C., 1989. *Comprehensive Organic Transformation: a Guide to Functional Group Preparations* 2nd ed. Wiley-VCH, New York.
- Mahata, N., Cunha, A.F., Orfao, J.J.M., Figueiredo, J.L., 2008. Hydrogenation of nitrobenzene over nickel nanoparticles stabilized by filamentous carbon. *Applied Catalysis A: General* 351, 204–209.
- Mahata, N., Cunha, A.F., Orfao, J.J.M., Figueiredo, J.L., 2009. Hydrogenation of chloronitrobenzenes over filamentous carbon stabilized nickel nanoparticles. *Catalysis Communication* 10, 1203–1206.
- Malla, P.B., Ravindranathan, P., Komarneni, S., Roy, R., 1991. Intercalation of copper metal clusters in montmorillonite. *Nature* 351, 555–557.
- Masson, J., Cividino, P., Court, J., 1997. Selective hydrogenation of acetophenone on chromium promoted Raney nickel catalysts. III. The influence of the nature of the solvent. *Applied Catalysis A: General* 161, 191–197.
- McFadden, S.X., Misha, R.S., Valiev, R.Z., Zhilyaev, A.P., Mukherjee, A.K., 1999. Low-temperature superplasticity in nanostructured nickel and metal alloys. *Nature* 398, 684–686.
- Mohapatra, S.K., Sonavane, S.U., Jayaram, R.V., Selvam, P., 2002. Regio- and chemoselective catalytic transfer hydrogenation of aromatic nitro and carbonyl as well as reductive cleavage of azo compounds over novel mesoporous NiMCM-41 molecular sieves. *Organic Letters* 4, 4297–4300.
- Pande, S., Saha, A., Jana, S., Sarkar, S., Basu, M., Pradhan, M., Sinha, A.K., Saha, S., Pal, A., Pal, T., 2008. Resin-immobilized CuO and Cu nanocomposites for alcohol oxidation. *Organic Letters* 10, 5179–5181.
- Puntes, V.F., Krishnan, K.M., Alivisatos, A.P., 2001. Molecular rulers for scaling down nanostructures. *Science* 291, 2115–2117.
- Qin, X.Y., Lee, J.S., Kim, J.G., 1999. Magnetic properties of nanostructured  $\gamma$ -Ni-46Fe alloy synthesized by a mechanochemical process. *Journal of Applied Physics* 86, 2146–2154.
- Rao, C.N.R., Kulkarni, G.U., Thomas, P.J., Edwards, P.P., 2000. Metal nanoparticles and their assemblies. *Chemical Society Reviews* 29, 27–35.
- Samec, J.S.M., Backvall, J.E., Anderson, P.G., Brandt, P., 2006. Mechanistic aspects of transition metal-catalyzed hydrogen transfer reactions. *Chemical Society Reviews* 35, 237–248.
- Sapkal, S.B., Shelke, K.F., Shingate, B.B., Shingare, M.S., 2009. Nickel nanoparticle-catalyzed facile and efficient one-pot synthesis of polyhydroquinoline derivatives via Hantzsch condensation under solvent-free conditions. *Tetrahedron Letters* 50, 1754–1756.
- Sharma, V.K., Yngard, R.A., Lin, Y., 2009a. Silver nanoparticles: green synthesis and their antimicrobial activities. *Advances in Colloid and Interface Science* 145, 83–96.
- Sharma, P., Bhorodwaj, S.K., Dutta, D.K., 2009b. Nickel nanoparticles: controlled size and morphology in mesoporous clay. *Journal of Scientific Conference Proceedings* 1, 40–43.
- Sun, S., Murray, C.B., Weller, D., Folks, L., Moser, A., 2000. Monodisperse FePt nanoparticles and ferromagnetic FePt nanocrystal superlattices. *Science* 287, 1989–1992.
- Tamura, M., Fujihara, H., 2003. Chiral Bisphosphine BINAP-Stabilized Gold and Palladium nanoparticles with small size and their Palladium nanoparticle-catalyzed asymmetric reaction. *Journal of the American Chemical Society* 125, 15742–15743.
- Tu, W.Y., Xu, B.S., Dongs, S.Y., 2006. Electrocatalytic action of nano-SiO<sub>2</sub> with electrodeposited nickel matrix. *Materials Letters* 60, 1247–1250.
- Ukisu, Y., Miyadera, T., 1997. Hydrogen-transfer hydrodehalogenation of aromatic halides with alcohols in the presence of noble metal catalysts. *Journal of Molecular Catalysis A: Chemical* 125, 135–142.
- Upadhyaya, T.T., Katdare, S.P., Sabde, D.P., Ramaswamy, V., Sudalai, A., 1997. Chemoselective transfer hydrogenation of nitroarenes, aldehydes and ketones with propan-2-ol catalysed by Ni-stabilized zirconia. *Chemical Communications* 1119–1120.
- Wallis, P.J., Gates, W.P., Patti, A.F., Scott, J.L., Teoh, E., 2007. Assessing and improving the catalytic activity of K-10 montmorillonite. *Green Chemistry* 9, 980–986.
- Wang, M., Li, H., Wu, Y., Zhang, J., 2003. Comparative studies on the catalytic behaviors between the Ni–B amorphous alloy and other Ni-based catalysts during liquid phase hydrogenation of acetonitrile to ethylamine. *Materials Letters* 57, 2954–2964.
- Wang, L., Lu, A., Wang, C., Zheng, X., Zhao, D., Liu, R., 2006. Nano-fibriform production of silica from natural chrysotile. *Journal of Colloid and Interface Science* 295, 436–439.